

Generation of optical combs in a whispering gallery mode resonator from a bichromatic pump

Dmitry V. Strekalov and Nan Yu

*Jet Propulsion Laboratory, California Institute of Technology,
4800 Oak Grove Drive, Pasadena, California 91109-8099*

(Dated: January 26, 2023)

We report an experimental realization of a frequency comb arising from a whispering gallery mode resonator pumped by two optical frequencies. Two externally excited resonator modes couple due to Kerr nonlinearity to initially empty modes and give rise to new frequency components. This process is much more efficient than the previously reported single-pump four-wave mixing. As a result, only a few milliwatt pump is required to generate strong secondary fields. In further contrast with the single-pump approach, this process is thresholdless, so the secondary frequency components can efficiently generate those of higher orders and so on, in a cascade process leading to an optical comb.

PACS numbers: 42.60.Da, 42.65.Ky, 42.65.Hw

Optical resonators with high quality factor Q are routinely used in nonlinear optics. Optical parametric oscillators and cavity-enhanced second harmonic generation are perhaps the most common applications of optical resonators in conjunction with optical nonlinearity. Recently, a new similar application has emerged: generation of the optical frequency combs [1, 2]. Optical combs found their applications as optical clocks and frequency standards of extremely high accuracy [3], including those for astronomy [4] and molecular spectroscopy [5, 6]. They have also been proposed for use in quantum information processing [7, 8]. One method to generate optical combs is via four-wave mixing in a resonator with Raman or Kerr nonlinearity [9, 10, 11, 12, 13]. In this case the comb arises from direct or cascaded frequency conversion processes, which requires very high effective nonlinearities. The latter was achieved by using the whispering gallery mode (WGM) resonators, known for extremely high Q factors, reaching 5×10^{10} in crystalline materials [14].

The underlying physical process of Kerr-based optical comb generation is the degenerate four-wave mixing, also known as hyperparametric conversion. In this process two pump photons of the same mode are converted into a quantum-correlated Stokes and anti-Stokes photon pair, such that the total energy is conserved. The energy diagram of this process is shown in Fig. 1(a). To excite this process in a WGM resonator, the pump has to exceed a certain threshold power P_{th} , inversely proportional to the Q^2 [15]. In a resonator with linear mode spectrum this process will populate the adjacent to the pump pair of modes as well as those two, three, etc., of the resonator free spectral ranges (FSR) Ω away from the pump. The spectral range is therefore limited by the resonator dispersion, which eventually will make the excitation of distant pairs of modes incompatible with the energy conservation.

We realized a different, non-degenerate configuration of four-wave mixing comb by using two pumps coupled to two WGMs one or several FSRs apart. Then instead of coupling two vacuum and two pump fields (of the same mode), we have the leading-order coupling between three

pump fields and one vacuum field. For example, on the energy diagram in Fig. 1(b) two pump photons with frequency ω_1 are absorbed, and one pump photon with frequency $\omega_2 > \omega_1$ is emitted, along with the Stokes photon with $\omega_- = 2\omega_1 - \omega_2$. A symmetric process will lead to generation of the anti-Stokes photon with the frequency $\omega_+ = 2\omega_2 - \omega_1$. Since the pump field is usually much stronger than the new fields, the non-degenerate four-wave mixing is expected to be much more efficient than the degenerate. Furthermore, as we will see below, the non-degenerate process is thresholdless. It occurs at any pump power, which allows one to avoid the undesirable high-power effects such as thermorefractive oscillations [15] and stimulated Raman scattering. The high efficiency and absence of the threshold in the studied process leads us to expect that the newly generated frequency components will efficiently generate further components, spreading into a comb.

Our experimental setup diagram is shown in Fig. 1(c). We used a fluoride resonator with $\Omega = 13.56$ GHz. This material has nearly flat dispersion at the wavelength of 1.5 micron, so the resonator spectrum around this wavelength is highly equidistant. Light was coupled in and out of the resonator using two optical fibers polished at the optimal coupling angle [16]. The light from the input fiber reflected off of the resonator rim was collected by a photodetector to observe the spectrum of the resonator.

The input fiber combined light from two lasers centered at around 1560 nm. Both laser frequencies were simultaneously scanned around the selected WGMs of the same family, however separated by one, two, three or ten FSRs. This was achieved by fine-tuning each laser frequency offset until the selected resonances overlap on the oscilloscope screen. The resonator quality factor $Q = 7 \times 10^7$ was made relatively low to increase the linewidth and therefore the time both lasers are simultaneously coupled into their WGMs. The optical spectrum analyzer (OSA) connected to the output fiber was continuously acquiring data, asynchronously with the lasers scan. The instrument was set to retain the peak power values, therefore a trace recorded for a sufficiently long period of time re-

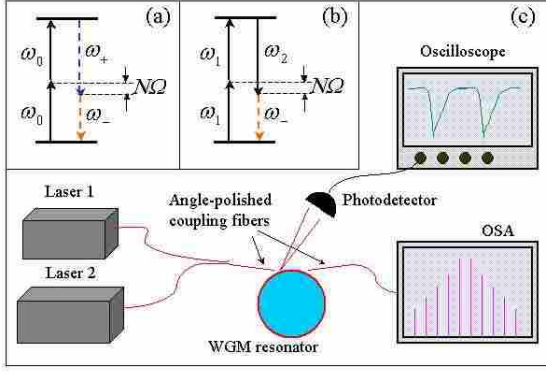


FIG. 1: Energy diagrams of previously (a) and presently realized (b) four-wave mixing processes generating a frequency comb. The experimental setup (c).

flected the situation with both lasers maximally coupled to the WGMs.

First, we set the lasers one FSR apart and recorded several traces for different pump powers. A typical trace observed at $P_1 = P_2 = 2.9$ mW is shown in Fig. 2. The two central peaks in this figure correspond to the pumps. Their output power is considerably lower than the input mainly because of weak output coupling (so as not to overload the resonator), but also because of linear and nonlinear loss. We measured this “insertion loss” at a low pump power, when the nonlinear loss is small, and found it to be approximately 35 dB (a factor of 3000). We will take this factor into account when comparing the experimental data with the theory.

We did not see any threshold pump power for the nonlinear oscillations. The power of the first-order new optical components as a function of the pump power is shown in Fig. 3 together with the theoretical curve, whose form is discussed below. This curve, which does not have any free curve-fitting parameters, approximates the data very well for the low pump power, but then fails. This probably happens because of the pump depletion when the low-power approximation is no longer valid.

We then repeated the same measurement separating the lasers by two, three and ten FSR. We had to stop at the ten FSR separations, because the lasers could not be tuned further. No significant difference between these measurements and the first one was observed. A comb spectrum corresponding to the ten FSR separation and the pump power $P_1 = P_2 = 4.75$ mW is shown in Fig. 4, together with the theoretical envelope of the comb.

Our experiment can be described in the framework of the general theoretical model of Kerr Hamiltonian coupling the WGMs, which has been discussed in [15] in detail. The difference in the present treatment is that the partial degeneracy of the Hamiltonian in [15] is removed,

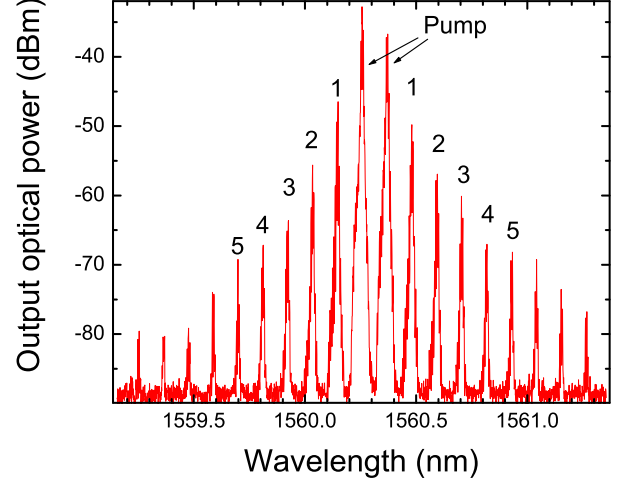


FIG. 2: A typical spectrum of four-wave mixing in a fluoroite WGM resonator. The two highest peaks correspond to the two pumps, each of 2.9 mW at the input. The numbers indicate the order of the new frequency components.

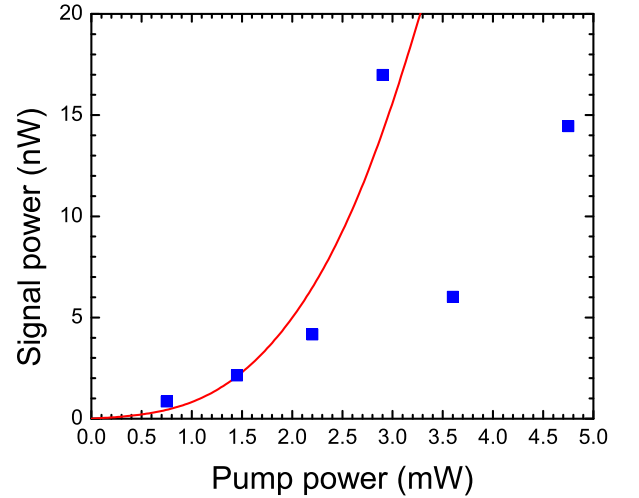


FIG. 3: Power of the first-order frequency component as a function of the pump power: the data and the theoretical curve.

and the leading-order process is a four-mode interaction rather than three-mode. The Hamiltonian $H = H_0 + V$ describing our system includes the following terms:

$$\begin{aligned} H_0 &= \hbar\omega_a a^\dagger a + \hbar\omega_b b^\dagger b + \hbar\omega_c c^\dagger c + \hbar\omega_d d^\dagger d, \\ V &= -\hbar\frac{g}{2} : (a + b + c + d + h.c.)^4 :, \end{aligned} \quad (1)$$

where $\omega_c < \omega_a < \omega_b < \omega_d$ are the eigenfrequencies of the equally spaced optical cavity modes, and c , a , b , and d are

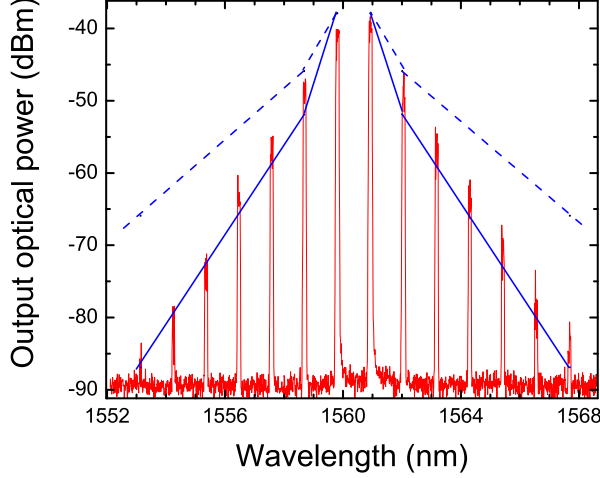


FIG. 4: The spectrum for $P_1 = P_2 = 4.75$ mW and 10 FSR (135.6 GHz) pump separation. The solid line is the comb envelope found theoretically without any free curve-fitting parameters. The dashed line is the envelope for the doubled pump power.

the annihilation operators for these modes, respectively. The coupling constant g is found in [15]:

$$g = \omega \frac{n_2}{n_0} \frac{\hbar \omega c}{\mathcal{V} n_0}, \quad (2)$$

where n_2 is the Kerr nonlinearity of the resonator material, n_0 is its refraction index and \mathcal{V} is the mode volume.

Notice that the fields represented by the operators a and b are strong pump fields, while the fields represented by c and d are initially vacuum fields. In Hamiltonian (1) we will only retain the leading terms with at least three pump fields operators. The equations of motion then take on the following form:

$$\begin{aligned} \dot{a} &= -i\omega_a a + 6ig(a^\dagger aa + 2ab^\dagger b + 2a^\dagger bc + bbd^\dagger), \\ \dot{b} &= -i\omega_b b + 6ig(b^\dagger bb + 2ba^\dagger a + 2b^\dagger ad + aac^\dagger), \\ \dot{c} &= -i\omega_c c + 6igaab^\dagger, \\ \dot{d} &= -i\omega_d d + 6igbba^\dagger. \end{aligned} \quad (3)$$

Following the steps of [15] we introduce the Langevin forces and write the system (3) in the stationary state as

$$\begin{aligned} \gamma a &= 6ig(a^\dagger aa + 2ab^\dagger b + 2a^\dagger bc + bbd^\dagger) + f_a, \\ \gamma b &= 6ig(b^\dagger bb + 2ba^\dagger a + 2b^\dagger ad + aac^\dagger) + f_b, \\ \gamma c &= 6igaab^\dagger + f_c, \\ \gamma d &= 6igbba^\dagger + f_d, \end{aligned} \quad (4)$$

where the loss rate γ and optical frequency ω are assumed to be the same for all modes, and

$$\langle f_{a,b} \rangle = \sqrt{\frac{2\gamma P_{a,b}}{\hbar \omega}}, \quad \langle f_{c,d} \rangle = 0. \quad (5)$$

Let us neglect the self- and cross-phase modulation terms in the first two equations (4). Then for the averaged amplitudes we find

$$\langle a \rangle = \sqrt{\frac{2P_a}{\gamma \hbar \omega}}, \quad \langle b \rangle = \sqrt{\frac{2P_b}{\gamma \hbar \omega}}, \quad (6)$$

$$\langle c \rangle = \frac{6gP_a\sqrt{P_b}}{\gamma} \left(\frac{2}{\gamma \hbar \omega} \right)^{3/2}, \quad (7)$$

$$\langle d \rangle = \frac{6gP_b\sqrt{P_a}}{\gamma} \left(\frac{2}{\gamma \hbar \omega} \right)^{3/2}. \quad (8)$$

Using Eq. (6) as the connection between the internal field and external power coupled to the resonator, which is also valid for the generated fields if we assume critical coupling, we finally arrive at

$$P_c = P_b \left(\frac{P_a}{P_{sat}} \right)^2, \quad P_d = P_a \left(\frac{P_b}{P_{sat}} \right)^2, \quad (9)$$

$$P_{sat} \equiv \frac{\gamma^2 \hbar \omega}{12g} = \frac{2\pi \mathcal{V}}{3n_2 \lambda} \left(\frac{n_0}{4Q} \right)^2 \approx \frac{1}{18} P_{th}, \quad (10)$$

where P_{th} is the threshold power for the single-pump hyperparametric oscillations, introduced in [15]. As the pump power approaches the P_{sat} , one may expect all of the comb components to have equal amplitude. However in our model the new fields are assumed to be weak compared to the pump. Outside of this approximation, the pump depletion as well as self- and cross-phase modulation need to be taken into account.

Let us point out that P_{sat} is much lower than the hyperparametric oscillations threshold P_{th} . Assuming $\lambda = 1.56 \mu\text{m}$, $n_0 = 1.44$, $n_2 = 3.2 \cdot 10^{-16} \text{ cm}^2/\text{W}$, $Q \approx 7 \cdot 10^7$, $\mathcal{V} \approx 10^{-4} \text{ cm}^3$, we find for our resonator $P_{sat} \approx 110$ mW. The experimental value of the P_{sat} can be found from the low-power measurements, when the weak secondary fields approximation underlying the result (9) is still valid. At $P_a = P_b = P = 1.5$ mW we measure the power ratio of the first-order component (see Fig. 2) to the pump $P^{(1)}/P \approx 250$ for one FSR separation; $P^{(1)}/P \approx 320$ for two FSR separation; and $P^{(1)}/P \approx 200$ for three FSR separation, where $P^{(1)} = P_c = P_d$. These values are reasonably close together considering the accuracy of the measurements. Taking their average we find from (9) $P_{sat} \approx 24$ mW. This value is lower than our theoretical estimate by a factor of 4.6. However, given a large uncertainty in both measured Q and estimated \mathcal{V} , we could expect only such an order-of-magnitude agreement. In the following analysis, we will use the experimental value of P_{sat} .

We showed that the four wave mixing with two pump frequencies does not have an oscillation threshold. Oscillations in the modes c and d occur at any pump power. This distinguishes it from the degenerate four-wave mixing (hyper-parametric) process. The significance of this distinction is that the two-pump process can be efficiently cascaded, while each excited mode plays the role of a new

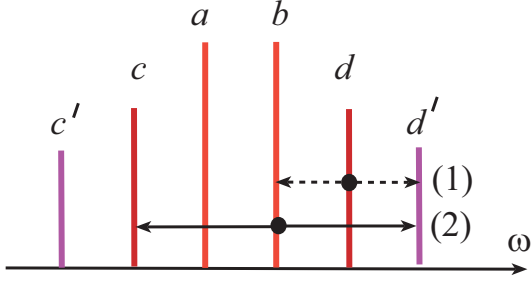


FIG. 5: Two possible channels of generating the second order component d' .

pump. The relative powers of thus generated higher order frequency components can be found from Eq. (9). We have already used it in a form $P^{(1)}/P = (P/P_{sat})^2$ to determine the experimental value of P_{sat} and to plot the theoretical curve in Fig. 3, which was scaled down by the “insertion loss” factor to be compared with the output power data. The second-order components c' and d' can now be generated in two ways each. For example, d' can be generated from b and d coupling across one FSR, or from c and b coupling across two FSRs, see Fig. 5. The second channel is more efficient, according to Eq. (9). This gives us the scaling law $P^{(2)}/P = (P/P_{sat})^3$. Continuing this analysis, we find the general scaling law for the comb:

$$\frac{P^{(n)}}{P} = \left(\frac{P}{P_{sat}} \right)^{n+1}, \quad (11)$$

which means that the number of observable frequency components grows very rapidly with the pump power. Notice that we only went as high as $0.2P_{sat}$ to get the

spectrum shown in Fig. 4. The comb envelopes shown in this figure was found using the experimental value of the P_{sat} and the scaling law (11). Notice that the observed frequency peaks consistently exceed the theoretical envelope. This happens for the same reason the theoretical curve fails to approximate the data in Fig. 3 at higher pump power. As the pump begins to deplete, the envelope (referenced to the pump level) is effectively lowered with respect to the rest of the comb.

To summarize, we have demonstrated a new and highly efficient method of generating optical combs in WGM resonators with Kerr nonlinearity. Even with a relatively low- Q resonator multiple new frequency components have been observed at a few milliwatt of the external CW pump power. Another interesting aspect of our method is that it allows one to choose the comb spacing as an integer number of the resonator FSRs. We demonstrated the comb spacing varying from one to ten FSR without any appreciable change in the relative power of the sidebands or the overall efficiency. This suggests that the spacing could in principle be made much larger. Variable lines spacing of the comb may not be only technically convenient for the spectroscopy applications, but also may partially compensate the resonator dispersion, which is the main factor limiting the comb span. We also would like to point out an interesting possibility of creating Moire comb pattern, by using three or more unequally spaced pump frequencies. This may enable an interesting approach to optical synthesizers.

The research described in this paper was carried out by the Jet Propulsion Laboratory, California Institute of Technology, under a contract with the National Aeronautics and Space Administration. D.V.S. also thanks Drs. Andrey Matsko of OEwaves and Ivan Grudinin of Caltech for helpful discussions.

-
- [1] T. Udem, R. Holzwarth, and T.W. Hansch, *Nature* **416**, 233-37 (2002).
 - [2] J. Ye and S.T. Cundiff, eds. *Femtosecond optical frequency comb technology*. (Springer, New York, 2005).
 - [3] L. Ma, Z. Bi, A. Bartels, L. Robertsson, M. Zucco, R. Windeler, G. Wilpers, C. Oates, L. Hollberg, and S.A. Diddams, *Science*, **303**, 1843-1845, (2004).
 - [4] Chih-Hao Li et al., *Nature* **452**, 610-612 (2008).
 - [5] M.J. Thorpe, K.D. Moll, J.J. Jones, B. Safdi, and J. Ye, *Science* **311**, 1595-99 (2006).
 - [6] S.A. Diddams, L. Hollberg, and V. Mbele, *Nature* **445**, 627-630 (2007).
 - [7] H. Zaidi, N.C. Menicucci, S.T. Flammia, R. Bloomer, M. Pysher, and O. Pfister, *Las. Phys.* **18**, 659 (2008).
 - [8] N.C. Menicucci, S.T. Flammia, and O. Pfister, *ArXiv quant-ph/0804.4468* (2008).
 - [9] S.M. Spillane, T. J. Kippenberg, and K. J. Vahala, *Nature* **415**, 621 (2002).
 - [10] A. A. Savchenkov, A. B. Matsko, D. V. Strekalov, M. Mohageg, V.S. Ilchenko and L. Maleki, *Phys. Rev. Lett.* **93**, 24395 (2004).
 - [11] T. J. Kippenberg, S.M. Spillane, and K. J. Vahala, *Phys. Rev. Lett.*, **93**, 083904 (2004).
 - [12] P. DelHaye, A. Schliesser, O. Arcizet, T. Wilken, R. Holzwarth and T. J. Kippenberg, *Nature*, **450**, 1214-17 (2007).
 - [13] A.A. Savchenkov, A.B. Matsko, V.S. Ilchenko, I. Solomatine, D. Seidel, and L. Maleki, *arXiv:0804.0263v1* (2008).
 - [14] I. Grudinin, A. Matsko, A. Savchenkov, D. Strekalov, V. Ilchenko, and L. Maleki, *Opt. Comm.*, **265**, 33-38 (2006).
 - [15] A. B. Matsko, A. A. Savchenkov, D. Strekalov, V. S. Ilchenko and L. Maleki, *Phys. Rev. A* **71**, 033804 (2005).
 - [16] V. S. Ilchenko, X. S. Yao, and L. Maleki, *Opt. Lett.* **24**, 723-725 (1999).